



Published in final edited form as:

J Neurosci. 2013 February 27; 33(9): 3834–3843. doi:10.1523/JNEUROSCI.3689-12.2013.

Identification of non-visual photomotor response cells in the vertebrate hindbrain

David Kokel^{1,2}, Timothy W. Dunn³, Misha B. Ahrens³, Rüdiger Alshut⁵, Chung Yan J. Cheung^{1,2}, Louis Saint-Amant^{*}, Giancarlo Bruni^{1,2}, Rita Mateus^{1,2}, Tjakko J. van Ham^{1,2}, Tomoya Shiraki⁴, Yoshitaka Fukada⁴, Daisuke Kojima⁴, Jing-Ruey J. Yeh¹, Ralf Mikut⁵, Johannes von Lintig⁶, Florian Engert³, and Randall T. Peterson^{1,2}

¹Cardiovascular Research Center and Division of Cardiology, Department of Medicine, Massachusetts General Hospital, Harvard Medical School, 149 13th Street, Charlestown, Massachusetts, 02129, USA

²Broad Institute, 7 Cambridge Center, Cambridge, Massachusetts 02142, USA

³Department of Molecular and Cellular Biology, Harvard University, Cambridge, MA, USA

⁴Department of Biophysics and Biochemistry, Graduate School of Science, The University of Tokyo, 7-3-1 Hongo, Bunkyo-ku, Tokyo 113-0033, Japan

⁵Institute for applied Computer Science, Karlsruhe Institute of Technology, Karlsruhe, Germany

⁶Department of Pharmacology, School of Medicine, Case Western Reserve University, Cleveland, Ohio 44106, USA

Abstract

Non-visual photosensation enables animals to sense light without sight. However, the cellular and molecular mechanisms of non-visual photobehaviors are poorly understood, especially in vertebrate animals. Here, we describe the photomotor response (PMR), a robust and reproducible series of motor behaviors in zebrafish that is elicited by visual wavelengths of light, but does not require the eyes, pineal gland or other canonical deep-brain photoreceptive organs. Unlike the relatively slow effects of canonical non-visual pathways, motor circuits are strongly and quickly (seconds) recruited during the PMR behavior. We find that the hindbrain is both necessary and sufficient to drive these behaviors. Using *in vivo* calcium imaging, we identify a discrete set of neurons within the hindbrain whose responses to light mirror the PMR behavior. Pharmacological inhibition of the visual cycle blocks PMR behaviors, suggesting that opsin-based photoreceptors control this behavior. These data represent the first known light-sensing circuit in the vertebrate hindbrain.

Introduction

How the nervous system senses and responds to light is a fundamental question in neuroscience. Photobiology has traditionally focused on visual pathways (Ridge et al.,

2003). However, non-visual photo-sensation also plays an important role in animal physiology and behavior (Lucas et al., 1999; Berson et al., 2002; Hattar et al., 2003; Zaidi et al., 2007; Nosedá et al., 2010). The majority of research on non-visual photic behaviors has been dedicated to understanding circadian rhythms, which are controlled via hormones over relatively long timescales (hours to days) (Reppert and Weaver, 2001). Beyond circadian rhythms, non-visual pathways can also control motor behaviors on a short time scale (seconds) (Becker and Cone, 1966; Harth and Heaton, 1973; Heaton and Harth, 1974; Peirson et al., 2009). For example, it has been recently shown that deep brain photoreceptors control light-seeking behaviors in zebrafish larvae (Fernandes et al., 2012). Such behaviors are a fundamental aspect of how the vertebrate nervous system responds to light, but remain poorly understood at the cellular and molecular level.

The retina is the only known light-detecting organ in mammals. However, some birds and reptiles express specialized extraocular photoreceptors in various organs including the pineal complex, deep brain, and skin (Yoshikawa et al., 1998; Vigh et al., 2002). A number of photopigments have been identified in these extra ocular tissues, including pinopsin (Okano et al., 1994; Max et al., 1995), melanopsin (Provencio et al., 1998), parapinopsin (Blackshaw and Snyder, 1997), exo-rhodopsin (Mano et al., 1999), vertebrate-ancient opsin (Val-opsin) (Kojima et al., 2000) and neuropsin (Nakane et al., 2010). These opsins are thought to enable non-visual photodetection (Vigh et al., 2002). However, their precise roles in physiology and behavior are poorly understood. Here, we have investigated the phenotypic, cellular and molecular mechanisms of the zebrafish photomotor response behavior using a combination of genetic, behavioral, electrophysiological and calcium imaging techniques. We find an unexpected circuit in the zebrafish hindbrain that is required for non-visual light-driven motor behaviors. These data implicate a new locus of photosensitive hindbrain neurons controlling non-visual light detection and motor behaviors in vertebrates.

METHODS

Fish maintenance and aquaculture

Zebrafish embryos were collected from group mating wild type zebrafish (Ekkwill). Embryos, of either sex, were raised in HEPES (10 mM) buffered E3 media in a dark incubator at 28 °C.

Behavioral recordings and data analysis

Grouped—The PMR assay was performed as described (Kokel et al., 2010). Briefly, groups of 8–10 embryos were distributed into the wells of flat bottom black 96 well plates. 1000 frames of digital video were recorded at 30 fps. The motion index was calculated by frame differencing. ‘Excitation scores’ are calculated by taking the 75th percentile of the motion index during indicated phases of the PMR behavior. Measurements and analysis were performed using the Metamorph and Matlab software packages.

Individual—To quantify individual zebrafish movements, we developed an image-processing pipeline with the following steps: Gaussian Deblurring was used to reduce

camera noise. Hough Circle Detection was used to identify a region of interest (ROI) around the chorion surrounding each embryo. The ROI for each animal is dynamically tracked through all video frames. Movement is quantified by frame differencing and normalized relative to the ROI intensity. Manual inspection the movies revealed that high magnitude, low frequency peaks in the motion index correlated with coiling events in the movies, so these peaks were defined as coiling events by the algorithm. Similarly, low magnitude high frequency peaks correlated with swimming events, so these peaks were defined as swimming by the algorithm. Coiling events within swimming events were also detected. Videos were processed using the MATLAB software package and the open source MATLAB Toolbox Gait-CAD (Mikut, 2008). The total calculation time of the whole processing pipeline including fish finding, tracking and classification does not exceed 1.5 minutes for each movie on a usual desktop computer. We also developed a standalone graphical user interface providing easy application, batch processing of the video data as well as automated report generation. The software is available from the authors upon request.

Statistical analysis—We used one-way ANOVA and the Tukey HSD post hoc test to test for significant differences between groups, generate 95% confidence intervals and identify groups with significantly different means. For groups with significant differences, we used the two-tailed t-test to test the null hypothesis and calculate the *p* value. Statistical analyses were performed using the *anova1*, *multcompare* and *ttest2* functions provided by the MATLAB statistics toolbox. All error bars represent standard deviations, unless otherwise noted.

Morpholino gene knockdown

All MOs in this study were obtained from GeneTools LLC (Corvallis, OR). Morpholinos used for this study were: valA(5'-TTTGT GAAGA CCTTT CTGAG TTTGC-3'), valB(5'-TATAT GACTA ACCTT TCTGA GCTTC-3'), valB2(5'-GAGTG TTCGA TACCT ATTAA GCATA-3'), exorho(5'-CGGTGTTGTAGTGTGCTCACC GCCG-3'), opn4.1 (CTCTCCATGAAGAGTGATGGCTCAT), opn4b (CAGCCCTGTCCATACACAACACACA) and opn4xb (ACATCCTGAAAACACACACAGAGAA). Morpholino efficacy was verified by PCR identification of splicing defects in the targeted genes, except for the opn4.1 morpholino, which targets the opn4.1 ATG translations start site. The yolks of single cell stage fertilized embryos were injected with 1nL of the 0.5mM morpholino solutions (5 ng per animal) or as noted.

Confocal analysis

Live imaging of embryonic zebrafish brain was performed as previously described (Lowery and Sive, 2005). Briefly, zebrafish embryos were embedded in 0.7% low melting agarose. The agarose enabled movements to be visualized in digital videos while preventing animals from swimming away. Images were captured on an inverted microscope (AxioObserver Z1; Zeiss) using the LSM700 scanning system (Zeiss, 488-nm laser lines) and a 20x objective (Zeiss). Embryos globally expressed a GFP transgene (Krovel and Olsen, 2002) to enable their visualization under the 488-nm laser stimulus illumination.

Photoc stimuli

Light stimuli were generated with a 300-watt xenon bulb housed in a Sutter Lambda LS illuminator and delivered to the well 10s and 20s (or 13s and 23s) after the start of each video. A cold mirror (reflectance between 300 nm and 700 nm) on the Sutter illuminator was used to block wavelengths outside of this range. Stimulus wavelengths were restricted using a quadband beamsplitter (Semrock; DA/FI/TR/Cy5-4X4M-B-ZHE) and four single band exciters (center wavelength/bandwidth): 387/11, 485/20, 560/25 and 650/13 (Semrock, Brightline FF01). Light intensity was measured using a PM100D power meter attached to a S120VC photodiode power sensor (Thorlabs). Intensity of the full strength white light stimulus on the embryos was $67 \mu\text{W}/\text{mm}^2$. The intensities of violet (387nm) and red (650nm) wavelengths were $3 \mu\text{W}/\text{mm}^2$. The intensities of blue (485nm) and green (560nm) wavelengths were $15 \mu\text{W}/\text{mm}^2$. High intensity violet (405nm; $600 \mu\text{W}/\text{mm}^2$) and red (650nm; $23 \mu\text{W}/\text{mm}^2$) stimuli were generated with pen style laser pointers ($<5\text{mW}$), and their intensities were reduced using neutral density filters. For comparison, ambient light in the laboratory was $\sim 1 \mu\text{W}/\text{mm}^2$ and direct sunlight on rare sunny day in Boston was $667 \mu\text{W}/\text{mm}^2$.

Dissections and spinalized preparations

Dissections were performed under the same general conditions as described (Downes and Granato, 2006). To remove the eyes and pineal gland, the zebrafish hindbrain was severed between the anterior hindbrain ventricle and the otic vesicle, at approximately the level of rhombomere 3–4, completely removing all midbrain and forebrain structures including the eyes and pineal complex (Asaoka et al., 2002). Data were collected 1hr-3hr post surgery, however the decapitated preparations were surprisingly robust, responding to stimuli for >12 hours post transection. Surgeries were performed under the microscope with forceps and a sharp razor blade following brief ice anesthesia. Dissected preparations were prepared and maintained in 1X Ringer's solution (116 NaCl, 2.9 KCl, 1.8 CaCl₂, 5 HEPES, pH 7.2; in mM).

Electrophysiology

We devised a 14-minute recording protocol in which we recorded from a muscle cell in partially paralyzed embryos aged 32 to 36 hpf. Lights were turned off at the beginning of the recording and the responsiveness of the embryos to photo and tactile stimuli was assessed. Most of the embryos also showed spontaneous fictive motor activity during the period of dark adaptation (11/15).

Myocyte recordings were obtained from embryos aged 32–36 hours at room temperature using methods previously described (Hamill et al., 1981; Ribera and Nusslein-Volhard, 1998; Drapeau et al., 1999). Embryos were anesthetized by adding Tricaine (0.02% w/v) to our Evans extracellular recording solution (mM): 134 NaCl, 2.9 KCl, 2.1 CaCl₂, 1.2 MgCl₂, 10 glucose, 10 HEPES, adjusted to pH 7.8 with NaOH. The embryos were pinned to a 35mm Sylgard coated dish and the skin overlying several somites was removed. The solution was replaced by gravity perfusion (1–2 mls/sec) of anesthetic-free Evans which contained $6\mu\text{M}$ d-tubocurarine in order to partially paralyze the preparation and enable recording from muscle cells under the whole cell patch clamp configuration. The internal

recording solution contained (in mM): 116 K-gluconate, 16 KCl, 2 MgCl₂, 10 HEPES, 10 EGTA, at pH 7.2 with KOH to which we added 0.1% SulforhodamineB for cell identification. Borosilicate glass electrodes had resistances of 4–6 MΩ when filled with internal recording solution. Recordings were made with an Axopatch 200B amplifier (Axon Instruments, Union City, CA) low pass filtered at 2 kHz and sampled at 10kHz. The microscope used was a Zeiss examiner A1 and fine pipette movement was controlled with a Sutter MPC-200 manipulator system. Tactile stimuli were delivered by ejecting solution from a pipette with a 25 micron opening where the pressure and duration were set via a picospritzer III (Parker). Photo stimuli were delivered using the built in illumination from the microscope (100W) where the duration was limited at 1 second using a uniblitz shutter (Optikon) triggered by a TTL pulse, this illumination was enhanced with a camera flash (Vivitar, 600 CR) occurring at the beginning of the 1 second TTL triggered time period. Data acquisition and TTL triggering of stimuli were achieved with pClamp 10 software using a Digidata 1440A interface. The initial data analysis was done with Clampfit 10, and figures were prepared using Adobe Illustrator.

Calcium imaging

A custom built two-photon microscope (Denk et al., 1990) was used to monitor neuronal activity in the hindbrain of 32–38 hpf zebrafish. The embryos expressed the genetically encoded calcium indicator GCaMP2 under the pan-neuronal HuC promoter, and were homozygous nacre in a WIK wild type background. Embryos were treated in phenylthiourea (PTU) in order to remove pigmentation and were pre-screened before imaging for robust responses to photic stimuli. Embryos were then dechorionated and paralyzed by bathing them in 1 mg/ml bungarotoxin (Invitrogen) solution and creating a small lesion at the tip of the tail with a forceps for better access to the internal tissues. Paralyzed embryos were side-mounted in 2% agarose and covered in standard E3 fish water in preparation for imaging. During imaging experiments, one second of blue light was delivered by an LED (Thorlabs) 3 times at 30s intervals. This was repeated for the next imaging plane with a 12 minute delay in order to allow the PMR to recover. Because of leakage of the blue light to the photomultiplier tube (PMT), the PMT was switched off during blue light stimulation, so that measurement of GCaMP2 fluorescence commenced upon offset of the stimulus.

Fluorescence movies were analyzed with custom written Matlab software as described (Ahrens et al., 2012). First, a square ROI, half the size of a neuron, is swept over all locations of the imaging plane. At each location, a fluorescence time-series, averaged over the ROI, is extracted and converted to a statistic for the ‘peaky-ness’ of the fluorescence signal at that point. If $f(x,y,t)$ is the fluorescence of the pixel at x, y at time t , and $f_{\text{squ}}(x,y,t)$ is the average fluorescence of the box centered at pixel x, y , and f_{avg} is the average fluorescence over space and time for the entire image sequence, then the statistic was defined to be

$$m(x, y) = \langle [f_{\text{squ}}(x, y, t) / \langle f_{\text{squ}}(x, y, t) \rangle + f_{\text{avg}}] ^ 3 \rangle$$

where $\langle \dots \rangle$ denotes the average over t . This measure was chosen because it bears resemblance to the usual dF/F but contains an offset to counteract the undesired amplification of noise; the third power was chosen because it nonlinearly converts peaks in the fluorescence signal to larger values of the statistic. This measure — one of several tested — yielded spatial signal maps $m(x,y)$ which tended to be at least as sensitive as sets of ROIs selected manually from observation of the raw and dF/F movies. These signal maps were thresholded and points of interest were found at the approximate centers of the peaks of $m(x,y)$ by first smoothing with a two-dimensional Gaussian and then finding the local maxima of the smoothed map. These formed the centers of the final ROIs (see Fig. 5E). These ROIs were then checked manually for any obvious artifacts. For the representative slice shown in Fig. 5B, automatically detected ROIs were hand segmented to match the shape of each neuron associated with a given ROI. The regions indicated by dotted red lines contain many detected ROIs that were associated with fiber tracts rather than individual somata. For constructing the standardized ROI spatial distribution map, automatically detected ROIs from 4 fish with complete image stacks through at least one half of the brain were assigned coordinates relative to the location of the first occipital nerve in rhombomere 8. In this three dimensional coordinate system, each ROI was assigned a rostrocaudal distance along the ventral surface of the brain relative to the nerve, a dorsoventral distance along the line normal to its position on the previously defined rostrocaudal axis, and a mediolateral distance from the lateral edge of the brain. Each ROI was then plotted onto an average intensity projection of a standard 36 hpf brain. The density metric used in 5D was calculated by averaging ROI densities across all sampled imaging planes from three additional fish that were exposed to all three conditions. For each plane, ROI density was calculated by dividing the number of detected ROIs by the volume of labeled neurons in the plane (area of labeled neurons \times 1 μm).

RESULTS

The PMR is a stereotyped behavior of reproducible kinematic events

Recently, we discovered the photomotor response (PMR) — a robust series of motor behaviors triggered by photic stimuli in embryonic zebrafish (Kokel et al., 2010). In the PMR behavior, dark-adapted zebrafish embryos (30 hours post fertilization (hpf)) respond to a bright pulse of light with a striking series of stereotyped motor behaviors within the chorion (Fig. 1a). The PMR can be divided into different phases including background, excitation and inactive/refractory phases (Fig. 1a,b). Before the stimulus, individual animals move infrequently with spontaneous coiling movements (Fig. 1a,b). Then, the stimulus elicits vigorous motor excitation lasting for approximately 5–7s. Following excitation, the animals enter an inactive/refractory phase, characterized by less than background levels of activity and unresponsiveness to a second pulse of light (Fig. 1a, b). Interestingly, it takes approximately 10 minutes of dark re-adaptation between stimuli for animals to respond to a second pulse of light (Fig. 1b).

We find that individual animals undergoing the PMR exhibit at least two types of motor events — coiling and swimming — that can be discriminated based on visual inspection of behavioral recordings. Coiling describes large alternating contractions that are likely to be

analogous to turning events in older animals. By contrast, swimming describes high frequency contractions that serve to propel the animal in the forward direction. Using a custom image-processing algorithm to analyze the behavior of individual animals, we find that swimming and coiling events can be discriminated via the amplitude and duration of peaks in the motion. Coiling events correspond to large-magnitude low-frequency peaks, whereas swimming events correspond to low-magnitude high-frequency peaks (Fig. 1c).

Overall, we identified 1,540 coiling events and 19,775 swimming events in an analysis of 425 animals during the PMR behavior. The distribution of these events shows that motor activity increases dramatically following stimulus presentation (Fig. 1d). After a median of 2.2s following the start of the stimulus presentation, coiling frequency increases approximately 10-fold, from 0.07 coils/s to 0.82 coils/s, for a median duration of 0.8s. Swimming behaviors, which are only rarely observed prior to the stimulus in only 0.5% of animals, are observed in 38% of animals following the stimulus and last for a median duration of 3.3s (Fig. 1e,f). Interestingly, the peak of swimming behaviors occurs 1.75s after the peak of coiling behaviors, indicating the PMR excitation phase can be subdivided into an early period of rapid coiling, followed by a later period of prolonged swimming, although coils are not always followed by swimming (Fig. 1e,f). By the end of this excitation phase, coiling behaviors decrease to 0.02 coils/s, approximately 3-fold lower than background levels, and animals do not respond to a second pulse of light (Fig. 1b–d). These results indicate that the PMR behavior is a stereotyped series of reproducible coiling and swimming events followed by a long period of inactivity.

Motor circuits are strongly recruited during PMR excitation

To understand the mechanism underlying the series of coiling and swimming events that occur during the PMR, we devised a 14 minute electrophysiological recording protocol in which we recorded responses from a muscle cell in partially paralyzed embryos aged 32 to 36 hpf. Lights were turned off at the beginning of the recording and the responsiveness of the embryos to photo and tactile stimuli (tail or head) was assessed. Embryos were dark adapted for 10 minutes and then tested again with photo and tactile stimuli (Fig. 2). Consistent with our video analysis, we find two types of electrophysiological events during head-touch, tail touch and PMR assays—low frequency large amplitude events and high frequency low amplitude events—consistent with fictive coiling and swimming respectively (Fig. 2a). None of the embryos responded to the light stimuli before dark adaptation ($n=15$), whereas they all responded to tactile stimulation. Most of the embryos showed spontaneous fictive motor excitation during the period of dark adaptation (11/15). The mean latency to tail and head tactile stimulus responses were significantly different from each other at 27 ± 2 ms ($n=18$) and 38 ± 4 ms ($n=16$) respectively ($p<0.01$) while the mean latency of responses to photo stimulation in the same animals was a full two orders of magnitude greater than either head or tail latencies at $3,988 \pm 612$ ms ($n=14$, $p<0.001$) (Fig. 2b). This massive increase in latency suggests that the recruitment of the motor system by light stimulation may be dependent on a very slow cellular and/or molecular mechanism that is different from the mechanisms controlling the touch response. The photomotor response included a high percentage of fictive coils (92%, $n=18$), whereas spontaneous motor output consisted of 82% ($n=11$) fictive coils; head touch elicited fictive coils in 72% ($n=18$) of

determine if tail photoreceptors are necessary for the zebrafish PMR, we analyzed the PMR in animals lacking the caudal half of their bodies. Tailless animals exhibit a robust PMR, indicating that the tail is not necessary for PMR photo-sensation, and that PMR photoreceptors are not located exclusively in the tail (Fig. 3c).

Supraspinal input from the brain is not necessary for spontaneous coiling or touch evoked coiling behaviors in the zebrafish (Downes and Granato, 2006). To determine if the hindbrain is required for the PMR, we analyzed the behavior of spinalized animals. We find that spinalized preparations lacking the hindbrain, did not respond to photic stimuli (Fig. 3c). Thus, unlike the touch response, supraspinal input from the hindbrain is necessary for the PMR.

Because the hindbrain is necessary for the PMR, we wondered if it might also be sufficient for sensing photic stimuli. To test this hypothesis, we used confocal microscopy to restrict photic stimulation to the column of cells above and below the eye, hindbrain, trunk or tail. We find that motor activity is not elicited by photic stimuli restricted to the eye, trunk or tail (Fig. 3d). By contrast, PMR excitation is strongly and reproducibly elicited by photic stimuli directed at the hindbrain (Fig. 3d). Together, these data suggest that hindbrain neurons are both necessary and sufficient to elicit PMR behaviors.

The PMR is a response to visible light

To determine the relationship between stimulus intensity and response magnitude, we exposed dark-adapted animals to white light stimuli (300–700nm) from a xenon lamp at various intensities. Whereas $1 \mu\text{W}/\text{mm}^2$ is too dim to trigger PMR excitation, a $13 \mu\text{W}/\text{mm}^2$ stimulus elicits a significant increase in motor activity, $p < 0.001$ (Fig. 4a). Thus, the minimum intensity needed to trigger PMR excitation is between 1 – $13 \mu\text{W}/\text{mm}^2$. Stimulus intensities greater than or equal to $33 \mu\text{W}/\text{mm}^2$ trigger significantly more excitation than the minimum effective intensity, $p < 0.005$ (Fig. 4a). These data indicate that PMR behaviors are triggered by stimuli approximately 50X less intense than direct sunlight ($667 \mu\text{W}/\text{mm}^2$). Furthermore, these data suggest that PMR behaviors could be triggered by natural stimuli outside the laboratory.

To determine which wavelengths of light are sufficient to trigger the PMR, we exposed animals to violet (387nm), blue (480nm), green (560nm) and red (650nm) stimuli. We find that blue and green wavelengths (both approximately $15 \mu\text{W}/\text{mm}^2$) reproducibly trigger robust PMR excitation (Fig. 4b). By contrast, neither violet (405nm) nor red (650nm) stimuli ($15 \mu\text{W}/\text{mm}^2$ and $23 \mu\text{W}/\text{mm}^2$ respectively) trigger PMR excitation (Fig. 4b). These data suggest that the PMR is triggered by blue and green light stimuli, but not by shorter or longer wavelengths..

To determine the duration of light necessary to trigger PMR excitation we analyzed the behavior of animals exposed to blue light stimuli (480nm, $15 \mu\text{W}/\text{mm}^2$) for various durations. We find that the response magnitudes are the same for stimuli lasting 1s or 20s (Fig. 4c). Similarly, the maximum response duration is 5–7s, for stimuli lasting either 1s or 20s. A 5–7s response duration is also observed for bright ($67 \mu\text{W}/\text{mm}^2$) white stimuli lasting 1s or 20s (data not shown). These data indicate that PMR excitation has a finite magnitude

and duration, and does not continue under constant light. (Fig. 4d). Together, these data suggest that the minimum stimulus duration for maximum effect is approximately 1s.

In larval zebrafish, visual phototaxis behavior is triggered by changes in the relative intensities of field and target stimuli (Burgess et al., 2010). To determine if PMR behaviors are also triggered by relative changes in light intensity, we pre-adapted zebrafish embryos to low levels of ambient light ($1 \mu\text{W}/\text{mm}^2$) for 10 min prior to PMR analysis. Next, we exposed these light-adapted animals to a large relative increase in brightness. Surprisingly, even very intense stimuli ($67 \mu\text{W}/\text{mm}^2$) do not trigger PMR excitation in light adapted animals (Fig. 4a). Thus, unlike visual phototaxis, the PMR depends on dark adaptation, rather than relative changes in light intensity.

A discrete set of hindbrain neurons drive PMR behaviors

To understand which neurons in the brain may be activated during the PMR, we measured neuronal activity in transgenic zebrafish expressing the genetically encoded fluorescent calcium indicator GCaMP2 (Diez-Garcia et al., 2007) under the pan-neuronal HuC promoter (Park et al., 2000). By monitoring the neuronal fluorescence changes elicited by photic stimuli with two-photon laser scanning microscopy, we were able to identify the specific location of neurons involved in the PMR (Fig. 5a). In 7 responsive 32–38 hpf fish, neurons in the caudal hindbrain, but not in the forebrain or midbrain, showed robust excitation to the photic stimulus, consistent with the hypothesis that supraspinal input is necessary to drive PMR behaviors. Figure 5b shows that in one representative animal, 21 neurons and 2 distinct fiber tracts fire synchronously during the PMR, illustrating the common pattern of excitation in response to the photic stimulus (Fig. 5b). By pooling the normalized positions of identified regions of interest (ROIs) across responsive fish, we show that active neurons are distributed throughout the caudal hindbrain (Fig. 5E), with the highest frequency of active neurons in Ro8, $\sim 45\mu\text{m}$ caudal to the first occipital nerve (Fig. 5f, bottom, blue). ROIs also cluster with greatest frequency $35\mu\text{m}$ from the ventral surface on the brain (Fig. 5f, top right, orange) and $10\mu\text{m}$ from the lateral surface of the brain (Fig. 5f, top left, cyan). Some PMR-correlated neuronal activity was also observed in the anterior spinal cord (dashed line in Fig. 5e). All observed neuronal responses are likely to correspond to the PMR because activity is consistently locked to stimulus onset with a fixed latency and can only be observed following the first stimulus after a long refractory period. Across all identified ROIs, the median time to fluorescence onset was 2.5s, and the median duration of the calcium response was 6s (Fig. 5c), in close agreement with the latencies and durations of the coiling and swimming events that occur during PMR excitation (Fig. 1 and 2). When hindbrain activity is compared with forebrain activity during stimulus trials, a pronounced difference in both the density of identified ROIs and the amplitude of detected responses emerges (Fig. 5d). These data support the conclusion that the PMR stimulus specifically recruits neurons in the hindbrain. Furthermore, the density of responsive ROIs in the hindbrain during stimulus trials is significantly different from the density during no stimulus trials. These data reiterate that hindbrain responses during stimulus presentation are stimulus-evoked and not artifacts of the experimental preparation (e.g. two-photon scanning). The few hindbrain responses detected during no stimulus trials most likely reflect baseline spontaneous activity in hindbrain circuits. Note that due to limitations of the

calcium sensor, it remains possible that we are underestimating the number and distribution of responsive neurons. Nonetheless, the anatomical clustering of identified ROIs, coupled with the similarity of neuronal response and behavioral response parameters, suggests that a discrete set of hindbrain neurons drive PMR motor activity.

Opsins are necessary for the PMR

Vertebrate photosensation requires the opsins, a large family of retinal-based G protein coupled receptors (Peirson et al., 2009). To determine if neurons in the zebrafish hindbrain sense photic stimuli via opsin-based phototransduction, we analyzed the effects on opsin impairment on PMR behavior. The zebrafish genome encodes >10 extra-retinal opsins with different expression patterns and functions including at least 5 melanopsin isoforms (Matos-Cruz et al., 2011). We chose 3 candidate opsin genes for further analysis including exorhodopsin, valopsinA and valopsinB (Kojima et al., 2008). To determine if these candidate opsins are necessary for the PMR, we used anti-sense morpholinos to knock-down their expression. We find that PMR excitation is not reduced in the morphant animals, suggesting that these opsins are not necessary for PMR excitation (Fig 6a).

The visual retinoid cycle, depends on 11-*cis* retinal (Burns and Baylor 2001). To determine if the visual cycle is necessary for the PMR, we treated animals with the small molecule Ret-NH₂, which inhibits synthesis of 11-*cis*-retinal in the zebrafish (Schonthaler et al., 2007). We find that Ret-NH₂-treated animals fail to exhibit PMR behaviors including the PMR excitation and inactive phases (Fig 6b–d). Importantly, Ret-NH₂-treated animals appear otherwise normal, showing normal background motion and touch response. Melanopsin-based photoreception is independent of the visual retinoid cycle (Tu et al., 2006), suggesting that melanopsin is not necessary for PMR excitation. Because PMR excitation appears to depend on the visual cycle, these data suggest that the PMR is mediated by one or more opsins in the nervous system.

DISCUSSION

Here, we have described the molecular, cellular and behavioral mechanisms of the zebrafish photomotor response. The PMR behavior is the first photic behavior linked to light-sensitive neurons in the vertebrate hindbrain and the earliest known photic behavior to develop in the zebrafish. At least three attributes distinguish the PMR from other previously reported behaviors in the zebrafish. First, the PMR latency and refractory phases are orders of magnitude longer than those observed for other stimuli. For example, the previously reported latency and refractory periods for responses to acoustic, tactile and photic stimuli are milliseconds in duration (Saint-Amant and Drapeau, 1998; Burgess and Granato, 2007a, b; Best et al., 2008), whereas the PMR latency and refractory phases last for seconds and minutes, respectively. Second, the neuroanatomical requirements of the PMR are distinct from other behaviors that occur at this time in development. For example, supraspinal input is necessary for the PMR, unlike spontaneous coiling, touch evoked coiling, and touch evoked swimming (Downes and Granato, 2006). Finally, the PMR depends on non-ocular photoreceptors, unlike other photic behaviors such as the light adaptation response (Burgess

and Granato, 2007a), optokinetic response (Rick et al., 2000) and the visual-motor response (Emran et al., 2007).

It appears that the early zebrafish embryo has a limited repertoire of motor responses consisting of coils and swims, and that these motor responses can be differentially recruited by specific upstream circuits (Saint-Amant and Drapeau, 1998, 2000; Brustein et al., 2003). Whereas touch stimuli elicit brief coiling and swimming events, the PMR evokes coils and swims with long latency and long duration. Because hindbrain neurons link sensory input to motor output, they provide an excellent starting point for studying the underlying circuitry of this complex series of behaviors.

Most behavioral reflexes in the zebrafish have very short refractory periods (ms). By contrast, the minimum inter-stimulus-interval for maximum PMR excitation is several orders of magnitude longer (10 min). One possible explanation for this long refractory phase is opsin photobleaching. Most opsins utilize *cis-to-trans* isomerization of the retinaldehyde chromophore as the primary photoreceptive event and must regenerate the *cis* chromophore to regain photosensitivity. Recovery from photobleaching occurs over a similar timescale as the PMR refractory phase (10 min) (Sexton et al., 2012), suggesting that photobleaching may explain the 10 minute inter-stimulus interval between PMR excitation phases.

Different mechanisms may control the PMR excitation and inactive/refractory phases. We show that light stimuli inhibit spontaneous coiling activity at 27 hpf without eliciting PMR excitation. At 27 hpf, spontaneous coils are generated and propagated by an extensive network of neurons interconnected in the spinal cord by gap junctions (Saint-Amant and Drapeau, 2001). Spontaneous coils are independent of chemical synaptic transmission and are dependent on electrical coupling of the neuronal network within the spinal cord (Saint-Amant and Drapeau, 2001). At 27 hpf, inhibitory signals from the photomotor response cells may be sufficient to block spontaneous coiling. By 32 hpf, the nervous system may develop additional synaptic inputs that drive the PMR excitation phase. One possibility is that each phase may be controlled by independent photoreceptors..

Opsin-based phototransduction is based on photoisomerization of the chromophore 11-*cis*-retinal to *all-trans*-retinal. Chromophore regeneration, via the retinoid cycle, is necessary to restore photoreceptors to their dark-adapted state. The small molecule Ret-NH2 is a potent and selective inhibitor of chromophore regeneration (Golczak et al., 2005) that reduces levels of 11-*cis*-retinal in wild-type zebrafish (Schonthaler et al., 2007). We find that Ret-NH2 blocks PMR behaviors, suggesting that opsin-based phototransduction is necessary for these non-visual photic responses. However, exactly which opsin or opsins are necessary for PMR behaviors remains unclear. Morpholino knockdown of six candidate genes did not block the PMR, suggesting that an untested opsin or multiple redundant opsins may control PMR behaviors.

What adaptive purpose might the PMR serve for fish in the wild? Similar non-visual photic behaviors have been previously described in lampreys (Young, 1935), *C. elegans* (Edwards et al., 2008; Liu et al., 2010), and *Drosophila* (Xiang et al., 2010). In these animals, non-visual light-induced motor behaviors appear to function as an escape response, to keep

animals hidden from dangerous UV radiation or predators (Xiang et al., 2010). The PMR is likely to serve a different purpose in zebrafish, because it only occurs prior to hatching, when the chorion prevents animals from swimming away. One possibility is that the PMR is a consequence of irradiance detection mechanisms with alternative primary functions. For example, it may be useful for animals to modulate neuronal excitability based on environmental light levels. Alternatively, the PMR may be an evolutionarily vestige with important ancestral functions in other organisms. Overall, the PMR presents new opportunities to understand the development and function of vertebrate non-visual photobiology and may improve our understanding of how the nervous system responds to light.

Acknowledgments

We thank John Dowling and members of our research groups for encouragement and advice. This work was supported by NIH grants K01MH091449 (DK), R01MH086867 and R21MH085205 (RTP), DP1 NS082121 and R01DA030304 (T.W.D. and F.E.). This work was partly supported by Grants-in-Aid for Scientific Research from JSPS (to Y. F. and D.K.). T.W.D. was supported by the National Science Foundation Graduate Research Fellowship, M.B.A was supported by a Sir Henry Wellcome Postdoctoral Fellowship from the Wellcome Trust, and R.T.P. was supported by the Charles and Ann Sanders MGH Research Scholar award.

References

- Ahrens MB, Li JM, Orger MB, Robson DN, Schier AF, Engert F, Portugues R. Brain-wide neuronal dynamics during motor adaptation in zebrafish. *Nature*. 2012; 485:471–477. [PubMed: 22622571]
- Asaoka Y, Mano H, Kojima D, Fukada Y. Pineal expression-promoting element (PIPE), a cis-acting element, directs pineal-specific gene expression in zebrafish. *Proceedings of the National Academy of Sciences of the United States of America*. 2002; 99:15456–15461. [PubMed: 12438694]
- Becker HE, Cone RA. Light-stimulated electrical responses from skin. *Science*. 1966; 154:1051–1053. [PubMed: 5919759]
- Berson DM, Dunn FA, Takao M. Phototransduction by retinal ganglion cells that set the circadian clock. *Science*. 2002; 295:1070–1073. [PubMed: 11834835]
- Best JD, Berghmans S, Hunt JJ, Clarke SC, Fleming A, Goldsmith P, Roach AG. Non-associative learning in larval zebrafish. *Neuropsychopharmacology : official publication of the American College of Neuropsychopharmacology*. 2008; 33:1206–1215. [PubMed: 17581529]
- Blackshaw S, Snyder SH. Parapinopsin, a novel catfish opsin localized to the parapineal organ, defines a new gene family. *The Journal of neuroscience : the official journal of the Society for Neuroscience*. 1997; 17:8083–8092. [PubMed: 9334384]
- Brockerhoff SE, Hurley JB, Janssen-Bienhold U, Neuhauss SC, Driever W, Dowling JE. A behavioral screen for isolating zebrafish mutants with visual system defects. *Proceedings of the National Academy of Sciences of the United States of America*. 1995; 92:10545–10549. [PubMed: 7479837]
- Brustein E, Saint-Amant L, Buss RR, Chong M, McDearmid JR, Drapeau P. Steps during the development of the zebrafish locomotor network. *Journal of physiology, Paris*. 2003; 97:77–86.
- Burgess HA, Granato M. Modulation of locomotor activity in larval zebrafish during light adaptation. *The Journal of experimental biology*. 2007a; 210:2526–2539. [PubMed: 17601957]
- Burgess HA, Granato M. Sensorimotor gating in larval zebrafish. *The Journal of neuroscience : the official journal of the Society for Neuroscience*. 2007b; 27:4984–4994. [PubMed: 17475807]
- Burgess HA, Schoch H, Granato M. Distinct retinal pathways drive spatial orientation behaviors in zebrafish navigation. *Current biology : CB*. 2010; 20:381–386. [PubMed: 20153194]
- Denk W, Strickler JH, Webb WW. Two-photon laser scanning fluorescence microscopy. *Science*. 1990; 248:73–76. [PubMed: 2321027]
- Diez-Garcia J, Akemann W, Knopfel T. In vivo calcium imaging from genetically specified target cells in mouse cerebellum. *NeuroImage*. 2007; 34:859–869. [PubMed: 17161628]

- Downes GB, Granato M. Supraspinal input is dispensable to generate glycine-mediated locomotive behaviors in the zebrafish embryo. *Journal of neurobiology*. 2006; 66:437–451. [PubMed: 16470684]
- Drapeau P, Ali DW, Buss RR, Saint-Amant L. In vivo recording from identifiable neurons of the locomotor network in the developing zebrafish. *Journal of neuroscience methods*. 1999; 88:1–13. [PubMed: 10379574]
- Easter SS Jr, Nicola GN. The development of vision in the zebrafish (*Danio rerio*). *Developmental biology*. 1996; 180:646–663. [PubMed: 8954734]
- Easter SS Jr, Nicola GN. The development of eye movements in the zebrafish (*Danio rerio*). *Developmental psychobiology*. 1997; 31:267–276. [PubMed: 9413674]
- Edwards SL, Charlie NK, Milfort MC, Brown BS, Gravlin CN, Knecht JE, Miller KG. A novel molecular solution for ultraviolet light detection in *Caenorhabditis elegans*. *PLoS biology*. 2008; 6:e198. [PubMed: 18687026]
- Emran F, Rihel J, Adolph AR, Wong KY, Kraves S, Dowling JE. OFF ganglion cells cannot drive the optokinetic reflex in zebrafish. *Proceedings of the National Academy of Sciences of the United States of America*. 2007; 104:19126–19131. [PubMed: 18025459]
- Fernandes AM, Fero K, Arrenberg AB, Bergeron SA, Driever W, Burgess HA. Deep Brain Photoreceptors Control Light-Seeking Behavior in Zebrafish Larvae. *Current biology : CB*. 2012
- Golczak M, Kuksa V, Maeda T, Moise AR, Palczewski K. Positively charged retinoids are potent and selective inhibitors of the trans-cis isomerization in the retinoid (visual) cycle. *Proceedings of the National Academy of Sciences of the United States of America*. 2005; 102:8162–8167. [PubMed: 15917330]
- Hamill OP, Marty A, Neher E, Sakmann B, Sigworth FJ. Improved patch-clamp techniques for high-resolution current recording from cells and cell-free membrane patches. *Pflügers Archiv : European journal of physiology*. 1981; 391:85–100. [PubMed: 6270629]
- Harth MS, Heaton MB. Nonvisual photic responsiveness in newly hatched pigeons (*Columba livia*). *Science*. 1973; 180:753–755. [PubMed: 4702573]
- Hattar S, Lucas RJ, Mrosovsky N, Thompson S, Douglas RH, Hankins MW, Lem J, Biel M, Hofmann F, Foster RG, Yau KW. Melanopsin and rod-cone photoreceptive systems account for all major accessory visual functions in mice. *Nature*. 2003; 424:76–81. [PubMed: 12808468]
- Heaton MB, Harth MS. Non-visual light responsiveness in the pigeon: developmental and comparative considerations. *The Journal of experimental zoology*. 1974; 188:251–264. [PubMed: 4836187]
- Kojima D, Mano H, Fukada Y. Vertebrate ancient-long opsin: a green-sensitive photoreceptive molecule present in zebrafish deep brain and retinal horizontal cells. *The Journal of neuroscience : the official journal of the Society for Neuroscience*. 2000; 20:2845–2851. [PubMed: 10751436]
- Kojima D, Torii M, Fukada Y, Dowling JE. Differential expression of duplicated VAL-opsin genes in the developing zebrafish. *Journal of neurochemistry*. 2008; 104:1364–1371. [PubMed: 18036148]
- Kokel D, Bryan J, Laggner C, White R, Cheung CY, Mateus R, Healey D, Kim S, Werdich AA, Haggarty SJ, Macrae CA, Shoichet B, Peterson RT. Rapid behavior-based identification of neuroactive small molecules in the zebrafish. *Nature chemical biology*. 2010; 6:231–237.
- Krovel AV, Olsen LC. Expression of a vas::EGFP transgene in primordial germ cells of the zebrafish. *Mechanisms of development*. 2002; 116:141–150. [PubMed: 12128213]
- Liu J, Ward A, Gao J, Dong Y, Nishio N, Inada H, Kang L, Yu Y, Ma D, Xu T, Mori I, Xie Z, Xu XZ. *C. elegans* phototransduction requires a G protein-dependent cGMP pathway and a taste receptor homolog. *Nature neuroscience*. 2010; 13:715–722.
- Lowery LA, Sive H. Initial formation of zebrafish brain ventricles occurs independently of circulation and requires the *nanog* and *snakehead/atp1a1a.1* gene products. *Development*. 2005; 132:2057–2067. [PubMed: 15788456]
- Lucas RJ, Freedman MS, Munoz M, Garcia-Fernandez JM, Foster RG. Regulation of the mammalian pineal by non-rod, non-cone, ocular photoreceptors. *Science*. 1999; 284:505–507. [PubMed: 10205062]
- Mano H, Kojima D, Fukada Y. Exo-rhodopsin: a novel rhodopsin expressed in the zebrafish pineal gland. *Brain research Molecular brain research*. 1999; 73:110–118. [PubMed: 10581404]

- Matos-Cruz V, Blasic J, Nickle B, Robinson PR, Hattar S, Halpern ME. Unexpected diversity and photoperiod dependence of the zebrafish melanopsin system. *PLoS one*. 2011; 6:e25111. [PubMed: 21966429]
- Max M, McKinnon PJ, Seidenman KJ, Barrett RK, Applebury ML, Takahashi JS, Margolskee RF. Pineal opsin: a nonvisual opsin expressed in chick pineal. *Science*. 1995; 267:1502–1506. [PubMed: 7878470]
- Mikut, OB.; Braun, S.; Reischl, M. The open source Matlab toolbox Gait-CAD and its application to bioelectric signal processing. Proc, DGBMT-Workshop Biosignalverarbeitung; Potsdam. 2008. p. 109-111.
- Morris AC, Fadool JM. Studying rod photoreceptor development in zebrafish. *Physiology & behavior*. 2005; 86:306–313. [PubMed: 16199068]
- Nakane Y, Ikegami K, Ono H, Yamamoto N, Yoshida S, Hirunagi K, Ebihara S, Kubo Y, Yoshimura T. A mammalian neural tissue opsin (Opsin 5) is a deep brain photoreceptor in birds. *Proceedings of the National Academy of Sciences of the United States of America*. 2010; 107:15264–15268. [PubMed: 20679218]
- Nosedá R, Kainz V, Jakubowski M, Gooley JJ, Saper CB, Digre K, Burstein R. A neural mechanism for exacerbation of headache by light. *Nature neuroscience*. 2010; 13:239–245.
- Okano T, Yoshizawa T, Fukada Y. Pinopsin is a chicken pineal photoreceptive molecule. *Nature*. 1994; 372:94–97. [PubMed: 7969427]
- Park HC, Kim CH, Bae YK, Yeo SY, Kim SH, Hong SK, Shin J, Yoo KW, Hibi M, Hirano T, Miki N, Chitnis AB, Huh TL. Analysis of upstream elements in the HuC promoter leads to the establishment of transgenic zebrafish with fluorescent neurons. *Developmental biology*. 2000; 227:279–293. [PubMed: 11071755]
- Peirson SN, Halford S, Foster RG. The evolution of irradiance detection: melanopsin and the non-visual opsins. *Philosophical transactions of the Royal Society of London Series B, Biological sciences*. 2009; 364:2849–2865.
- Provencio I, Jiang G, De Grip WJ, Hayes WP, Rollag MD. Melanopsin: An opsin in melanophores, brain, and eye. *Proceedings of the National Academy of Sciences of the United States of America*. 1998; 95:340–345. [PubMed: 9419377]
- Reppert SM, Weaver DR. Molecular analysis of mammalian circadian rhythms. *Annual review of physiology*. 2001; 63:647–676.
- Ribera AB, Nusslein-Volhard C. Zebrafish touch-insensitive mutants reveal an essential role for the developmental regulation of sodium current. *The Journal of neuroscience : the official journal of the Society for Neuroscience*. 1998; 18:9181–9191. [PubMed: 9801358]
- Rick JM, Horschke I, Neuhauss SC. Optokinetic behavior is reversed in achiasmatic mutant zebrafish larvae. *Current biology : CB*. 2000; 10:595–598. [PubMed: 10837226]
- Ridge KD, Abdulaev NG, Sousa M, Palczewski K. Phototransduction: crystal clear. *Trends in biochemical sciences*. 2003; 28:479–487. [PubMed: 13678959]
- Saint-Amant L, Drapeau P. Time course of the development of motor behaviors in the zebrafish embryo. *Journal of neurobiology*. 1998; 37:622–632. [PubMed: 9858263]
- Saint-Amant L, Drapeau P. Motoneuron activity patterns related to the earliest behavior of the zebrafish embryo. *The Journal of neuroscience : the official journal of the Society for Neuroscience*. 2000; 20:3964–3972. [PubMed: 10818131]
- Saint-Amant L, Drapeau P. Synchronization of an embryonic network of identified spinal interneurons solely by electrical coupling. *Neuron*. 2001; 31:1035–1046. [PubMed: 11580902]
- Schmitt EA, Dowling JE. Early retinal development in the zebrafish, *Danio rerio*: light and electron microscopic analyses. *The Journal of comparative neurology*. 1999; 404:515–536. [PubMed: 9987995]
- Schonthaler HB, Lampert JM, Isken A, Rinner O, Mader A, Gesemann M, Oberhauser V, Golczak M, Biehlmaier O, Palczewski K, Neuhauss SC, von Lintig J. Evidence for RPE65-independent vision in the cone-dominated zebrafish retina. *The European journal of neuroscience*. 2007; 26:1940–1949. [PubMed: 17868371]

- Sexton TJ, Golczak M, Palczewski K, Van Gelder RN. Melanopsin is highly resistant to light and chemical bleaching in vivo. *The Journal of biological chemistry*. 2012; 287:20888–20897. [PubMed: 22547062]
- Tu DC, Owens LA, Anderson L, Golczak M, Doyle SE, McCall M, Menaker M, Palczewski K, Van Gelder RN. Inner retinal photoreception independent of the visual retinoid cycle. *Proceedings of the National Academy of Sciences of the United States of America*. 2006; 103:10426–10431. [PubMed: 16788071]
- Vigh B, Manzano MJ, Zadori A, Frank CL, Lukats A, Rohlich P, Szel A, David C. Nonvisual photoreceptors of the deep brain, pineal organs and retina. *Histology and histopathology*. 2002; 17:555–590. [PubMed: 11962759]
- Wakamatsu Y, Kawamura S, Yoshizawa T. Light-induced pigment aggregation in cultured fish melanophores: spectral sensitivity and inhibitory effects of theophylline and cyclic adenosine-3', 5'-monophosphate. *Journal of cell science*. 1980; 41:65–74. [PubMed: 6245098]
- White RM, Sessa A, Burke C, Bowman T, LeBlanc J, Ceol C, Bourque C, Dovey M, Goessling W, Burns CE, Zon LI. Transparent adult zebrafish as a tool for in vivo transplantation analysis. *Cell stem cell*. 2008; 2:183–189. [PubMed: 18371439]
- Xiang Y, Yuan Q, Vogt N, Looger LL, Jan LY, Jan YN. Light-avoidance-mediating photoreceptors tile the *Drosophila* larval body wall. *Nature*. 2010; 468:921–926. [PubMed: 21068723]
- Yoshikawa T, Okano T, Oishi T, Fukada Y. A deep brain photoreceptive molecule in the toad hypothalamus. *FEBS letters*. 1998; 424:69–72. [PubMed: 9537517]
- Young JZ. The photoreceptors of Lampreys: I. Light-sensitive Fibres in the Lateral Line Nerves. *J Exp Biol*. 1935; 12:229–238.
- Zaidi FH, Hull JT, Peirson SN, Wulff K, Aeschbach D, Gooley JJ, Brainard GC, Gregory-Evans K, Rizzo JF 3rd, Czeisler CA, Foster RG, Moseley MJ, Lockley SW. Short-wavelength light sensitivity of circadian, pupillary, and visual awareness in humans lacking an outer retina. *Current biology : CB*. 2007; 17:2122–2128. [PubMed: 18082405]
- Zimmerman. Cutaneous photoreception: a new sensory mechanism for reptiles. *Copeia*. 1990

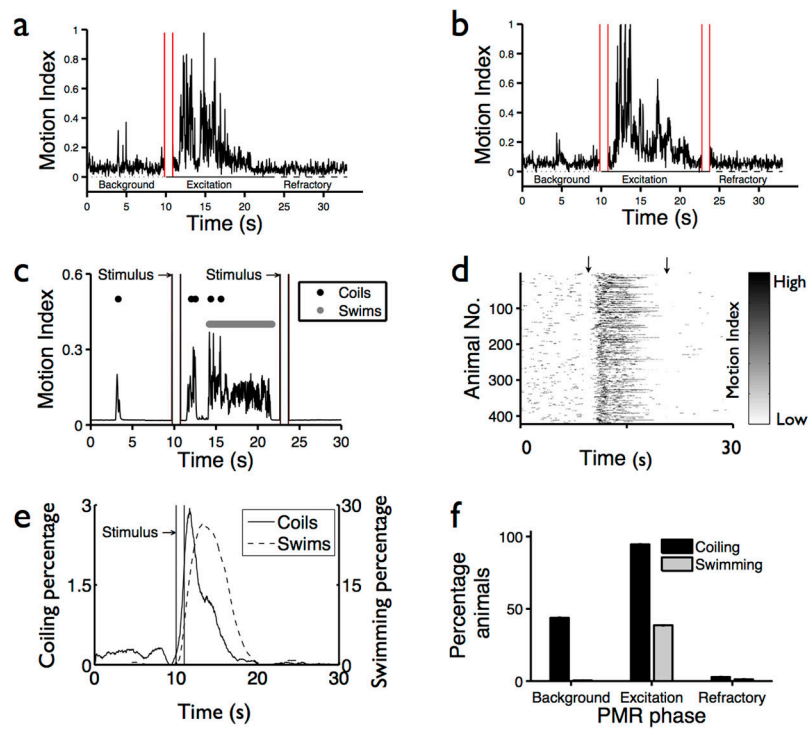


Figure 1.

Light stimuli elicit stereotyped photomotor behaviors in zebrafish embryos. Plots showing the combined motor activity of 10 dark-adapted zebrafish embryos in response to one (a) or two (b) light stimuli (red bars). (c) Plot showing the motor activity of an individual zebrafish during the PMR assay. High-magnitude-low-frequency peaks represent coiling events (filled circle), whereas low-magnitude-high-frequency peaks represent swim events (gray bar). Paired vertical lines at 10s and 23s are stimulus artifacts that indicate the start and end of each 1s stimulus. (d) Image showing the motor activity matrix of 479 individual animals. Matrix rows represent individual animals and columns represent time. Arrowheads indicate the timing of two 1s stimuli. (e) Smoothed histograms showing the probability of coiling (black) and swimming (gray) events for 479 individual animals during the PMR assay. (f) Barplot showing the percentage of animals exhibiting coiling and swimming behaviors (y-axis) during the indicated PMR phase (x-axis). The differences between the percentages of animals coiling during each phase are significant ($p < 0.001$). The percentage of animals swimming during the excitation phase is significantly more than during the background and refractory phases ($p < 0.001$).

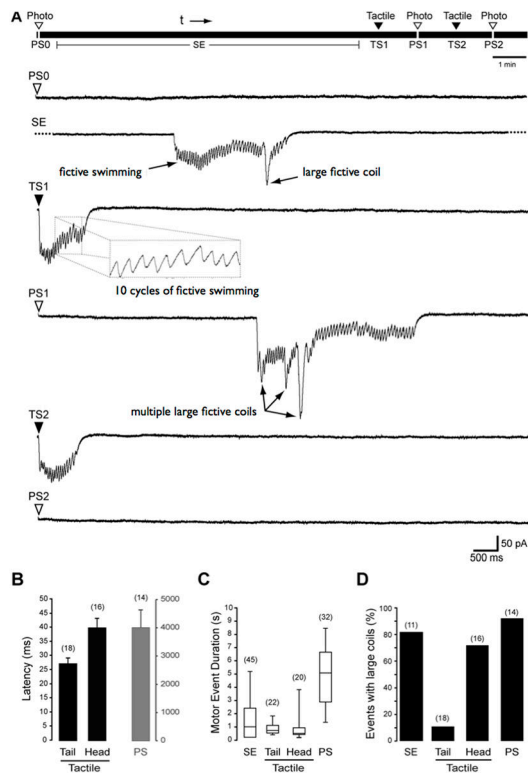


Figure 2.

Motor circuits are strongly recruited during PMR excitation. Muscle cells were recorded in paralyzed embryos to assay fictive motor output. (a) The top diagram shows the experimental procedure while the lines below show representative traces that begin upon stimulus triggering. Embryos are photostimulated at the beginning of the experiment (PS0), followed by 10 minutes of dark adaptation with occasional spontaneous events (SE), at the eleventh minute the embryos receive a tactile stimulus (TS1), followed by a photostimulus (PS1), another tactile stimulus (TS2) and a final photostimulus (PS2). (b) Latency graph for tail and head tactile stimuli and photo stimuli (PS). Note the 100-fold change in the grey axis. (c) Box-plot showing event duration for spontaneous, tactile and photo stimuli evoked events. (d) Percentage of events exhibiting large struggling coils in spontaneous, tactile and photo evoked events. The numbers in parentheses represent the total number of motor events analyzed.

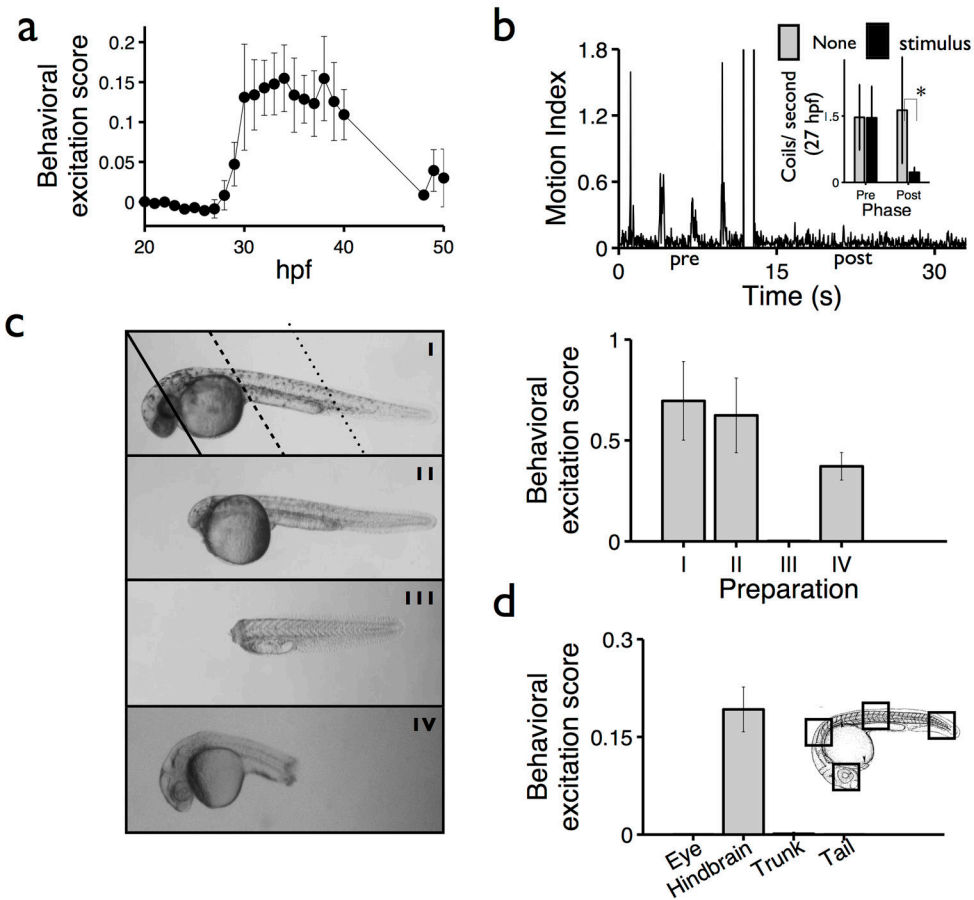
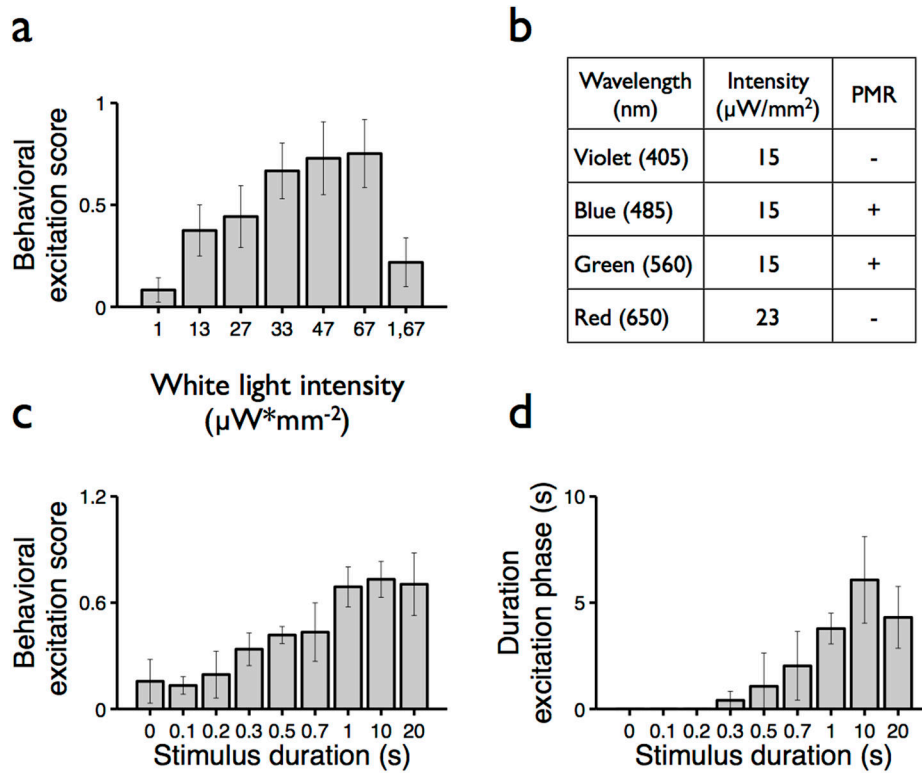


Figure 3.

The PMR is a non-visual photic behavior. (a) Lineplot showing behavioral excitation scores of animals tested at the indicated developmental ages ($n = 10$ wells). (b) The barplot quantifies average coils per second in 27 hpf animals before (pre) and after (post) stimulation ($n = 9$ animals per group). The difference between pre- and post-stimulation in light-treated animals is significant, $p < 0.01$ (*). The inset shows an example plot of reduced motor activity post-stimulation in a 27 hpf animal. (c) Images showing example preparations; upper panel. Preparation I is an intact animal. Solid, dashed and dotted lines indicate the locations of transections in panels II, III and IV. Preparation II lacks all forebrain and midbrain structures, but retains the posterior hindbrain. Preparation III lacks all supraspinal input but remains touch sensitive, and IV lacks a portion of the tail. Barplot showing behavioral excitation scores for the indicated preparations ($n = 5$ wells). Group III is significantly different from all other groups, $p > 0.001$. Note that reduced excitation score in tailless fish (type IV) is due to fewer moving pixels in these truncated animals. (d) Drawing of 30hpf zebrafish embryo showing stimulus locations (red boxes); upper panel. Barplot showing the behavioral excitation scores of animals stimulated at the indicated locations ($n = 3$ animals, each animal stimulated in every condition); lower panel. The difference between the group receiving hindbrain stimulation all other groups is significant, $p < 0.001$. All values are the mean and standard deviations.

**Figure 4.**

The PMR is a response to visible light. (a) Barplot showing behavioral excitation scores in response to white light stimuli (1s) at the indicated intensity ($n=10$). The difference between the groups treated with 1 and $13 \mu\text{W} \cdot \text{mm}^{-2}$ is significant, $p < 0.001$. Significantly more activity is elicited by $33 \mu\text{W} \cdot \text{mm}^{-2}$ than $13 \mu\text{W} \cdot \text{mm}^{-2}$, $p < 0.005$. “1, 67” indicates that these animals were pre-exposed to low levels of ambient light ($1 \mu\text{W}/\text{mm}^2$) for 10min prior to PMR analysis with a $67 \mu\text{W}/\text{mm}^2$ stimulus. (b) Table showing the effects of stimuli at the indicated wavelengths and intensities. Stimuli that trigger PMR excitation are indicated by (+), stimuli that did not are indicated by (-). (c) Barplot showing behavioral excitation scores in response to white light stimuli for the indicated stimulus duration ($n=5$). An analysis of variance showed that the differences between groups exposed to 0.5s or less are not statistically significant. There is a statistically significant difference between the 0.5s treatment group and the 1s, 10s and 20s treatment groups $p < 0.05$. The difference between 0.7s and 10s is also significant, $p < 0.05$ (d) Barplot showing the duration of behavioral excitation in response to stimuli of the indicated duration ($n=5$). The difference between the 0.1s and 20s treatment groups are significant, $p < 0.001$. All values are mean and standard deviations.

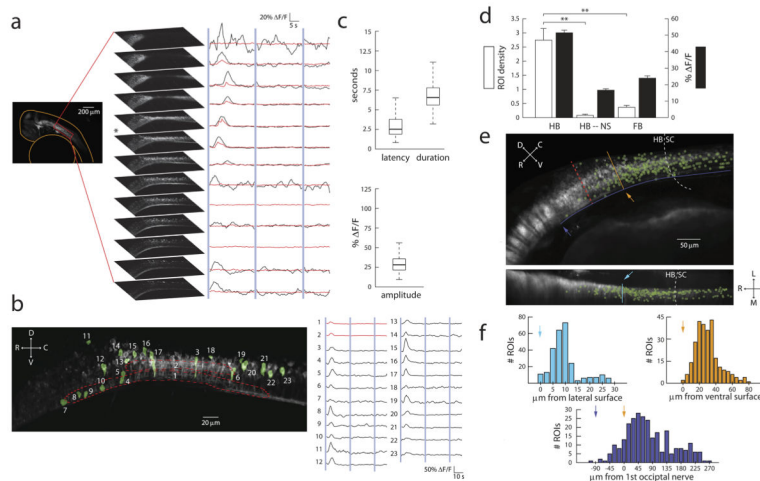


Figure 5.

A discrete set of neurons is activated during the PMR. (a) Left, three-dimensional projection of a typical 36 hpf embryonic zebrafish brain expressing GCaMP2 under the pan-neuronal HuC promoter. The orange outline denotes the anatomical border of the embryo. Right, 13 representative optical slices separated by 3 μm in the hindbrain region outlined in red. Neuronal responses to blue light stimulation (bars) are shown beside each slice. Red traces show the change in average fluorescence for the entire slice, black traces show the smoothed change in fluorescence for all active regions in the slice. (b) Activated neurons (green) and corresponding smoothed fluorescence changes from a single slice in the same embryo as (a). Traces 1 and 2 (red) show representative neuropil responses from the regions outlined by the dashed red lines. The image in (b) corresponds to the plane labeled with (*) in (a). (c) Boxplots showing the distribution of hindbrain neuronal response latencies, durations, and amplitudes during the PMR. ($n=318\text{--}328$ ROIs, 7 embryos). (d) Mean detected neuronal ROI densities (ROIs/ $1000 \mu\text{m}^3$, white) and response amplitudes (black) in the hindbrain (HB, 369 ROIs, 132 volumes) and forebrain (FB, 56 ROIs, 153 volumes) of three 36 hpf embryos. The same quantities are plotted for the hindbrain during trials without stimulus presentation (HB-NS, 11 ROIs, 132 volumes). Error bars depict standard error of the mean** denotes $p<0.001$, Student's t-test. (e) Top left, normalized spatial distribution of detected ROIs ($n=273$, green) from 4 fish overlaid on an average intensity projection of the hindbrain in a typical side-mounted 36 hpf HuC::GCaMP2 fish. Bottom left, the same spatial distribution of neurons as viewed from a top-down image reslice. (f) Top right, orange, histogram quantifying the spatial distribution of identified ROIs along the D-V axis. Top left, cyan, histogram quantification of M-L axis. Bottom, blue, R-C axis. Solid lines in (e) represent the axes used to construct corresponding histograms in (f). Arrows denote the starting positions along each axis used for histogram construction. Dotted white lines denote the hindbrain-spinal cord boundary. For reference, the dotted red line in (e) delineates the rostral extent of the image in (b).

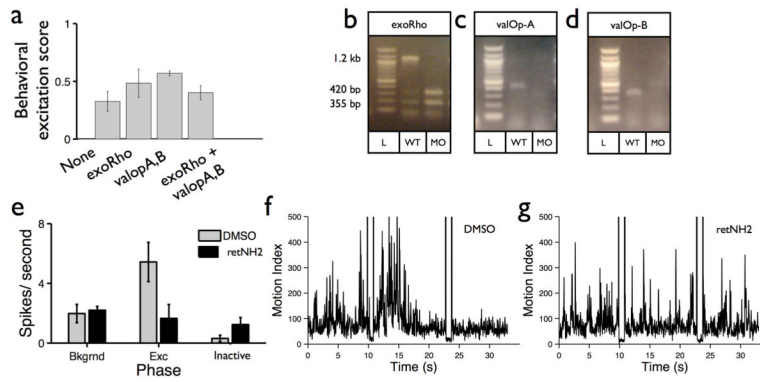


Figure 6.

Opsin phototransduction is necessary for photomotor excitation

(a) Barplot showing behavioral excitation scores of uninjected controls (None), and animals injected with morpholinos targeting exorhodopsin (exRho), valopsin A and valopsin B (valopA,B) and the three opsins together (exoRho + valopA,B) ($n=5$ wells, 10 animals per well). Morphant scores are not significantly less than the controls. (b–d) Gel images showing the efficacy of the splice blocking morpholinos tested in (a). (e) Barplot showing number of motion index spikes per second of animals treated with DMSO, or the opsin inhibitor retNH2 ($n=5$). For DMSO treated control animals, spike rate is significantly greater during the excitation phase (Exc) and significantly lower during the inactive phase (Inactive) as compared to background (Bkgrnd), $p<0.01$. For retNH2 treated animals, spike rate is not significantly different during any of the phases. Examples from animals treated with DMSO (f), or retNH2 (g) are shown.